

Variational quantum state diagonalization with computational-basis probabilities

Juan Yao^{1,2,3,*}

¹Shenzhen Institute for Quantum Science and Engineering,
Southern University of Science and Technology, Shenzhen 518055, Guangdong, China

²International Quantum Academy, Shenzhen 518048, Guangdong, China

³Guangdong Provincial Key Laboratory of Quantum Science and Engineering,
Southern University of Science and Technology, Shenzhen 518055, Guangdong, China

In this report, we propose a novel quantum diagonalization algorithm through optimizing a variational quantum circuit. The optimization process utilizes measurement outcomes in the computational basis to construct an objective function for variational optimization. Two distinct objective functions are introduced in this report. The first is constructed from the probabilities of 2^N computational basis states. By maximizing the sum of the squared diagonal elements of the evolved N -qubit quantum state, this function drives the state toward a diagonal form, with the optimized value corresponding to the purity of the input quantum state. To address the experimental challenges associated with measuring all 2^N basis states, we propose a second objective function based on N single-qubit measurement probabilities. This reduces measurement complexity with exponential growth, enhancing the feasibility of experimental implementation. In both cases, we explore the relationship between measurement probability distributions and the diagonalization of the evolved quantum state. Numerical simulations and analytical insights demonstrate that the variational optimization effectively transforms the input quantum state into its diagonalized form, offering a practical framework for quantum state diagonalization.

I. INTRODUCTION

Diagonalization is a fundamental theoretical tool used extensively in mathematics, physics, and machine learning. It simplifies mathematics operations such as computing matrix powers and exponentials [1]. In quantum mechanics, diagonalizing the Hamiltonian uncovers a system's eigenstates and energy levels, providing deep insights into its intrinsic properties [2]. In machine learning, diagonalization simplifies the representation of complex systems by decoupling complex dataset into manageable, independent components, which is core in dimensionality reduction and optimizing models [3]. Whether in the theoretical study of matrices in mathematics or practical applications in physics and machine learning, diagonalization serves as an invaluable tool for analysis and computation.

Classically, diagonalization typically involves finding the roots of the characteristic polynomial, which is mathematically effective but computationally expensive. Symbolic computation is feasible only for small matrices, where exact arithmetic can be applied efficiently. For larger matrices, numerical methods are usually employed. Standard classical numerical algorithms for diagonalization usually adopt iterative methods such as the QR decomposition algorithm [4], power iteration [5], and inverse iteration [6]. These methods iteratively approximate the eigenvalues and eigenvectors, providing solutions without the need to solve the characteristic polynomial analytically [7].

Quantum algorithms can solve certain problems exponentially faster than classical algorithms [8]. For instance, Shor's algorithm [9, 10] offers an efficient method for factoring large integers, a task that would require exponentially more time on a classical computer. Properties of superposition and entanglement enable quantum computers to explore multiple possibilities simultaneously, allowing them to perform parallel computations and significantly enhancing their power for specific tasks [8]. Implementations of quantum state di-

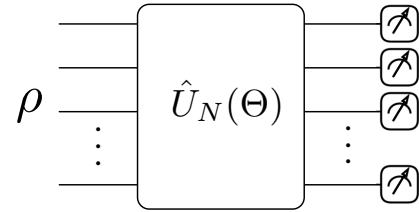


FIG. 1. The diagonalization of the input quantum state is realized through optimizing a variational quantum circuit. An N -qubit quantum state ρ is transformed using a parameterized unitary matrix $\hat{U}_N(\Theta)$. The evolved state $\rho' = \hat{U}_N \rho \hat{U}_N^\dagger$ is followed by a computational-basis measurement, which contributes to the objective function. By optimizing the parameters Θ according to the proposed objective function, the evolved state ρ' is automatically brought into a diagonal form.

agonalization have been explored in several studies [11–15]. However, most of these approaches focus primarily on approximating large eigenvalues. Ref. [12] proposes a variational method for constructing a diagonalizing unitary operator, where the cost functions are evaluated using diagonalized and partially diagonalized inner-product test circuits, which require two copies of the input density matrix. In contrast, we present a variational quantum diagonalization algorithm based on computational-basis probabilities, which significantly simplifies the evaluation process of the cost function.

As illustrated in Fig. 1, a variational quantum circuit [16] is applied to the input quantum state to facilitate its diagonalization. As a hybrid algorithm, the variational optimization process leverages classical optimization techniques to adjust the quantum circuit parameters [17]. We explore the relationship between the distribution of computational-basis probabilities and the diagonalized form of the evolved quantum state. By optimizing the proposed objective functions, which are based on measurement outcomes, the input quantum state can be fully diagonalized through an optimized unitary trans-

formation. In the following sections, we demonstrate the diagonalization process using two distinct objective functions. Notably, the second objective function relies exclusively on single-qubit measurement probabilities, thereby significantly reducing measurement complexity and enhancing the experimental feasibility of the quantum diagonalization algorithm.

II. GLOBAL COMPUTATIONAL-BASIS PROBABILITIES

As shown in the schematic diagram in Fig. 1, an N -qubit quantum state ρ undergoes a parameterized unitary transformation $\hat{U}_N(\Theta)$, resulting in the evolved state $\rho' = \hat{U}_N(\Theta)\rho\hat{U}_N^\dagger(\Theta)$. At the end of the circuit, a sufficient number of measurements are performed on ρ' in computational basis. Statistical analysis of the measurement outcomes provides the occupation probabilities for each computational basis with

$$p_{q_1, q_2, \dots, q_N} = \text{Tr}\{\rho' |q_1, q_2, \dots, q_N\rangle\langle q_1, q_2, \dots, q_N|\}, \quad (1)$$

where $|q_1, q_2, \dots, q_N\rangle$ denotes the computational basis state for N -qubit system, and q denotes 0 or 1 for each qubit. We parameterize the unitary transformation using elements of the Pauli group,

$$\hat{U}_N(\Theta) = e^{-i\theta_g \hat{P}_g}, \quad (2)$$

where \hat{P}_g represents an element of the Pauli group and is defined as

$$\hat{P}_g = \hat{\sigma}_{j_1} \otimes \hat{\sigma}_{j_2} \otimes \dots \otimes \hat{\sigma}_{j_N}, \quad (3)$$

with $\hat{\sigma}_j$ denotes the identity ($j = 0$) and the three Pauli matrices ($j = x, y, z$). The index g spans all possible configurations of $\{j_1, j_2, \dots, j_N\}$, excluding the trivial case where all $\hat{\sigma}_j$ are identity matrices. The set of variational parameters is given by $\Theta = \{\theta_g | g = 1, 2, \dots, 4^N - 1\}$. This universal parameterization ensures the expressivity for representing the diagonalizing transformation matrix.

To identify the parameters in the unitary transformation, we utilize the summation of the squared probabilities of the computational-basis states as the objective function, which is written as

$$\mathcal{D}(\Theta) = \sum_{q_1, q_2, \dots, q_N} p_{q_1, q_2, \dots, q_N}^2. \quad (4)$$

Noting that p_{q_1, q_2, \dots, q_N} is provided by the diagonal element of the evolved density matrix ρ' . When ρ' is fully diagonalized, the objective function \mathcal{D} becomes equivalent to the purity of the input state,

$$\mathcal{P} = \text{Tr}\{\rho'^2\}, \quad (5)$$

which is invariant under unitary transformations.

We simulate the optimization process using PyTorch [18] and PennyLane [19]. All data and code are available at [20]. Objective function \mathcal{D} given by Eq. (4) is used to optimize the parameters Θ in the unitary transformation, with the goal of maximizing \mathcal{D} using the Adam optimizer. The numerical

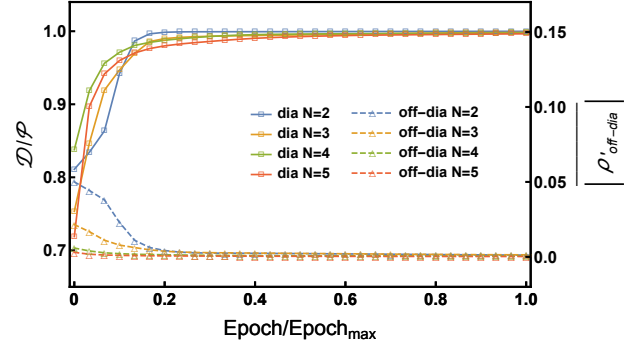


FIG. 2. Training results for the variational quantum circuit with the objective function \mathcal{D} for different qubit numbers N . (a) Throughout the optimization process, the ratio between objective function \mathcal{D} and purity \mathcal{P} is plotted over the training epochs as solid lines with square markers. (b) During training, $|\rho'_{\text{off-dia}}|$ is represented by a dashed line with triangular markers.

training results for different qubit numbers, $N = 2, 3, 4, 5$, are presented in Fig. 2. In the case where the input state is pure, the spectral decomposition simplifies to a single dominant eigenvalue, allowing the quantum state to be easily transformed into a product of single-qubit zero states [21]. Here, for each value of N , we randomly generate a mixed input quantum state, which includes finite off-diagonal elements. As shown in Fig. 2, the evolution of \mathcal{D} during training is plotted by the solid line with square markers. As the training progresses over a sufficient number of epochs, the objective function \mathcal{D} converges to its maximum, which corresponds to the expected purity value. During the training process, we also calculate the average amplitude of the off-diagonal elements of ρ' as follows:

$$\overline{|\rho'_{\text{off-dia}}|} = \frac{1}{2^N(2^N - 1)} \sum_{i \neq j} |\rho'_{ij}|, \quad (6)$$

which are plotted by the dashed lines with triangular markers. As illustrated in Fig. 2, at the end of each training, when $\mathcal{D} = \mathcal{P}$, all the off-diagonal elements vanish, indicating that the final state ρ' obtains a diagonal form. Note that neither the purity nor $|\rho'_{\text{off-dia}}|$ are directly accessed during the optimization process, nor are they required for the variation of the quantum circuit. Calculating purity and $|\rho'_{\text{off-dia}}|$ would typically involve quantum state tomography [22–24]. In our approach, however, only the objective function, provided by the computational-basis probabilities, is required for optimization, and \mathcal{D} can be estimated statistically through repeated measurement shots.

As illustrated by the numerical results in Fig. 2, by maximizing \mathcal{D} until it converges to the purity, we can transform the input quantum state into a diagonal form. This process reveals the eigenvalues and eigenvectors in quantum form: the probabilities of each computational basis state correspond to the eigenvalues of the input state, while the identified variational unitary provides the eigenvectors. In the following, we will analytically prove that \mathcal{D} is upper-bounded by the purity, and

when $\mathcal{D} = \mathcal{P}$, the associated quantum density matrix assumes a diagonal form with vanishing off-diagonal elements. Considering a general input quantum state ρ , which satisfies the Hermitian property $\rho = \rho^\dagger$, the purity can be calculated as

$$\mathcal{P} = \sum_{ij} \rho_{ij} \rho_{ji} = \sum_{ij} \rho'_{ij} \rho'_{ji} = \sum_i \rho'^2_{ii} + \sum_{i \neq j} \rho'_{ij} \rho'^*_{ij}, \quad (7)$$

where the second term is non-negative. This leads to the following inequality:

$$\mathcal{P} \geq \sum_i \rho'^2_{ii} = \mathcal{D}. \quad (8)$$

Here the equality holds if and only if all off-diagonal elements vanish, i.e., $\rho'_{i \neq j} = 0$.

In principle, the proposed variational quantum diagonalization algorithm can be implemented experimentally on a quantum platform. However, for a global computational basis, the measurement complexity increases exponentially with the number of qubits. For an N -qubit quantum state, the total number of computational basis states is 2^N . To achieve low statistical error in estimating the probabilities for all 2^N possibilities, the number of measurement shots required must be much larger than 2^N . As a result, for large N , obtaining accurate probability estimates for each computational basis becomes impractical. To address this issue, we propose a second objective function based on local computational basis.

III. LOCAL COMPUTATIONAL-BASIS PROBABILITIES

A. Single-qubit case

As an example, we consider the single-qubit case to demonstrate the process of diagonalizing the input quantum state, based on its single-qubit zero-state probability. An arbitrary single-qubit quantum state can be represented as a density matrix ρ with in the form of

$$\rho = \begin{bmatrix} \rho_{11} & \rho_{12} \\ \rho_{21} & \rho_{22} \end{bmatrix}. \quad (9)$$

Here, the property of Hermitian and normalization condition imply that $\rho_{12} = \rho_{21}^*$ and $\rho_{11} + \rho_{22} = 1$. A general unitary transformation for a single qubit can be parametrized as:

$$\hat{U}_{N=1}(\phi, \theta, \omega) = \begin{bmatrix} \cos \frac{\theta}{2} e^{-i \frac{\phi+\omega}{2}} & -\sin \frac{\theta}{2} e^{i \frac{\phi-\omega}{2}} \\ \sin \frac{\theta}{2} e^{-i \frac{\phi-\omega}{2}} & \cos \frac{\theta}{2} e^{i \frac{\phi+\omega}{2}} \end{bmatrix}, \quad (10)$$

where ϕ, θ, ω are the parameters that define the transformation. For optimization purposes, the objective function adopted here is the zero-state probability, defined as:

$$\pi = \text{Tr}[\rho' |0\rangle\langle 0|], \quad (11)$$

where ρ' is the evolved quantum state given by $\rho' = \hat{U} \rho \hat{U}^\dagger$. The probability π can be statistically estimated from outcomes of multiple measurement shots.

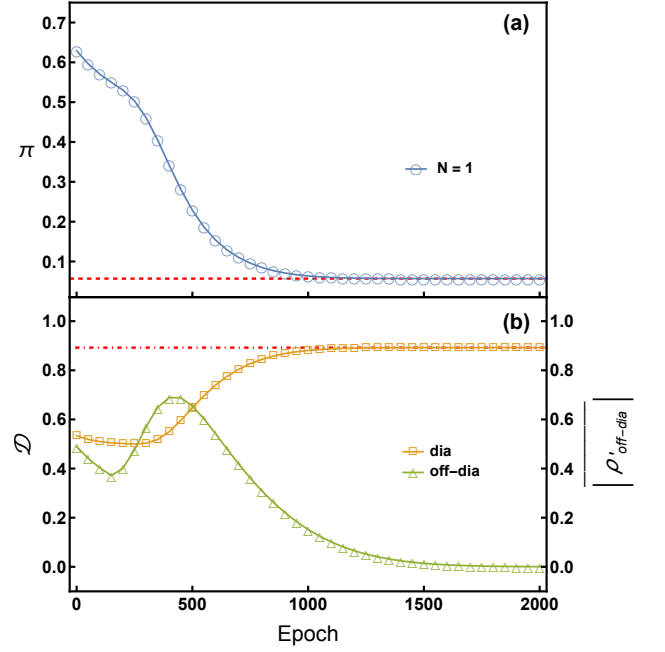


FIG. 3. Quantum diagonalization for an arbitrary $N = 1$ quantum state using the single-qubit zero-state probability as the objective function. (a) During training, the zero-state probability π is shown as a blue line with circular markers. The red dashed line represents the smaller eigenvalue of the input density matrix ρ . (b) During training, \mathcal{D} and $|\rho'_{\text{off-dia}}|$ are plotted as lines with square and triangular markers, respectively. The dot-dashed line indicates the purity \mathcal{P} of the input quantum state.

The training process is numerically simulated by optimizing the parameters $\{\theta, \omega, \phi\}$ in Eq. (10), with the goal of minimizing the objective function π of Eq. (11). As shown in Fig. 3 (a), the zero-state probability π decreases steadily throughout the training process, eventually converging to a minimum value. At the end of the process, the minimum value π_{\min} corresponds to the smaller eigenvalue of the input density matrix, as indicated by the red dashed line. To monitor the optimization process, we evaluate both \mathcal{D} in Eq. (4) and $|\rho'_{\text{off-dia}}|$ in Eq. (6), as shown in Fig. 3 (b). After optimization, \mathcal{D} saturates to the value of purity (orange line with squares), and all the off-diagonal elements of ρ' vanish (green line with triangles). This confirms that the evolved state ρ' attains a fully diagonal form by the end of the training process.

For the $N = 1$ case, the zero-state probability π is found to be bounded by the two eigenvalues of the input quantum state. When the input quantum state is pure, π spans its maximum range, varying from 0 to 1. Minimization of π will transform the input quantum state into state of $|1\rangle\langle 1|$. In contrast, for a mixed quantum state, the presence of mixture reduces the range of π . To analytically explore the relationship between the range of π and the evolution of the quantum state, the evolved quantum state ρ' can be explicitly derived, allow-

ing π to be expressed as (see more details in appendix A):

$$\begin{aligned} \pi(\theta, \phi) = & \frac{1}{2} + \frac{\rho_{11} - \rho_{22}}{2} \cos \theta \\ & - \frac{\rho_{12} + \rho_{21}}{2} \sin \theta \cos \phi \\ & - \frac{\rho_{12} - \rho_{21}}{2i} \sin \theta \sin \phi. \end{aligned} \quad (12)$$

Taking the derivatives of $\pi(\theta, \phi)$ with respect to θ and ϕ , the local extremal values are given by:

$$\pi^\pm = \frac{1}{2} \pm \sqrt{\frac{(\rho_{11} - \rho_{22})^2}{4} + \rho_{12}\rho_{21}}, \quad (13)$$

where \pm corresponds to the local maximal and minimal value, respectively. It can be verified that the two extreme values of π correspond to the two eigenvalues of the input density matrix ρ . The result indicates that both maximizing and minimizing the zero-state probability can realize a diagonalization of the input quantum state. At these extremes, the off-diagonal elements can be calculated as $\rho'_{12} = \rho'_{21} = 0$, ensuring that ρ' attains a diagonal form. The above proof indicates that the evolution of zero-state probability is constrained by two eigenvalues of the input quantum state. In addition, at the extremes, the evolved quantum state is diagonal.

B. Multi-qubit case

Given the intriguing results observed in single-qubit systems, it is reasonable to hypothesize that there exists a connection between the single-qubit probabilities and diagonalization of an N -qubit quantum state. Based on N single-qubit probabilities at zero state, we propose the following objective function for an N -qubit quantum state:

$$\mathcal{L} = \sum_{q=1}^N \sum_{n=1}^{N-q+1} \pi_q^n, \quad (14)$$

Here, π_q denotes the probability of the zero state for the q -th qubit, and n represents the allowed power index for the single-qubit probabilities. Within the summation, the highest degree of the polynomial is $n = N$, which involves only $\pi_{q=1}$. For $q = N$, the allowed power of the corresponding zero-state probability is only $n = 1$. When the system size $N = 1$, the objective function \mathcal{L} reduces to π_1 , as given by Eq. (11) for the single-qubit case. It is important to note that swapping any two qubits in the quantum state does not affect the optimization process. Therefore, the choices of \mathcal{L} are not unique for the optimization purpose.

To ensure the capability for diagonalization, a universal parameterization strategy can be adopted as given in Eq. (2). However, this approach involves multi-qubit interactions represented by the product of non-trivial Pauli matrices. For experimental implementation, various sufficiently expressive quantum circuit architectures can also be used [25, 26], provided they incorporate the desired diagonalizing unitary transformation. Here, we construct a hardware-efficient quantum

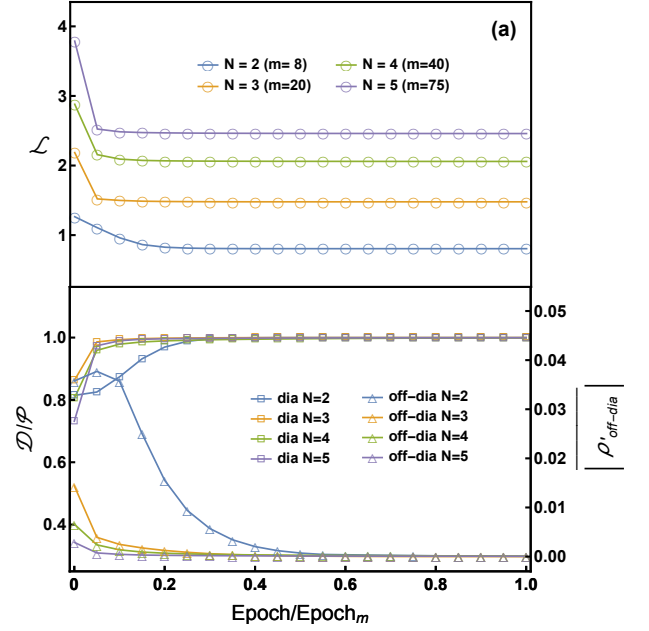


FIG. 4. Variation diagonalization results for various N -qubit quantum states with local computational-basis probabilities. (a) For each N , the objective function \mathcal{L} is plotted as a line with circular markers. m denotes the number of brick-wall building blocks for the corresponding quantum circuit. (b) For each optimization process, \mathcal{D} is shown as a line with square markers, while the average magnitude of off-diagonal elements $|\rho'_{\text{off-dia}}|$ is represented by a line with triangular markers.

circuit using a brick-wall architecture, denoted as $\hat{\mathcal{B}}(\Theta_j)$ [27]. The variational quantum circuit is constructed with m brick-wall building blocks, where the overall unitary transformation is given by $\hat{U}(\Theta) = \prod_{j=1}^m \hat{\mathcal{B}}(\Theta_j)$. The number of building blocks m required for each N is determined dynamically during the training process [27]. The depth of the quantum circuit is extended until the optimization of the objective function converges, at which point the minimal value of \mathcal{L} is reached in terms of m , as shown in Fig. 4 (a). As training progresses, as shown in Fig. 4 (b), the quantity $|\rho'_{\text{off-dia}}|$ becomes infinitesimally small, effectively vanishing all off-diagonal elements of the state. At this point, the diagonal form of the evolved state ρ' is confirmed by \mathcal{D} saturating to the purity \mathcal{P} . However, it is important to note that although the off-diagonal elements are vanishing, the eigenvalues of the quantum state have not been fully resolved. Additional operations will be needed to estimate the eigenvalues.

Compared to global measurement-based objective function \mathcal{D} of Eq. (4), the objective function \mathcal{L} relies on local measurements, requiring only single-qubit probabilities. For each qubit, only two degrees of freedom need to be statistically estimated. In contrast, for probabilities associated with the global computational basis, the number of degrees of freedom grows exponentially as 2^N . Therefore, especially for large N , the objective function \mathcal{L} , which is based on single-qubit probabilities, significantly reduces the measurement complexity [28].

IV. SUMMARY AND OUTLOOK

In this report, we propose variational quantum diagonalization algorithm with computational-basis probabilities. Building on the intrinsic connection between the evolution of measurement probabilities and the diagonalization of the quantum state, we introduce two objective functions for optimization. The second objective function based on local computational-basis probabilities significantly reduces measurement complexity, making experimental implementation more feasible.

However, for multi-qubit systems, a rigorous analytical understanding of \mathcal{L} is still lacking, despite its simple and elegant form. Further investigation is required to explore the connection between the local observables and the dynamics of an N -qubit quantum state. Nonetheless, this variational quantum state diagonalization algorithm could offer a promising approach for demonstrating quantum supremacy on near-term quantum hardware. [29, 30].

Acknowledgement. We thank Hui Zhai, Jiang Zhang, Youpeng Zhong, Zhigang Wu for helpful discussions. This work is supported by the Science, Technology and Innovation Commission of Shenzhen, Municipality (KQTD20210811090049034), Guangdong Basic and Applied Basic Research Foundation (2022B1515120021), and National Natural Science Foundation of China (Grant No. 11904190).

Appendix A: Detailed Calculations for the Optimization of π in the Single-Qubit Case

For single qubit case, the evolved state can be explicitly derived according to $\rho' = \tilde{U}\rho\tilde{U}^\dagger$ with $\tilde{U}_{N=1}$ parametrized by Eq. (10). The zero-state probability is given by the diagonal elements of ρ' with

$$\begin{aligned} \rho'_{11}(\theta, \phi) &= \frac{1}{2} + \frac{\rho_{11} - \rho_{22}}{2} \cos \theta \\ &\quad - \frac{\rho_{12} + \rho_{21}}{2} \sin \theta \cos \phi - \frac{\rho_{12} - \rho_{21}}{2i} \sin \theta \sin \phi, \end{aligned} \quad (\text{A1})$$

and the off-diagonal element is given by

$$\begin{aligned} \rho'_{12}(\theta, \phi, \omega) &= \frac{\rho_{11} - \rho_{22}}{2e^{i\omega}} \sin \theta + \rho_{12} \frac{1 + \cos \theta}{2e^{i\omega}} e^{-i\phi} \\ &\quad - \rho_{21} \frac{1 - \cos \theta}{2e^{i\omega}} e^{i\phi}. \end{aligned} \quad (\text{A2})$$

The first derivative of ρ'_{11} in terms of ϕ leads to

$$R \sin \theta \sin \phi = I \sin \theta \cos \phi, \quad (\text{A3})$$

where denoting $R = (\rho_{12} + \rho_{21})/2$ for the real part and $I = (\rho_{12} - \rho_{21})/2i$ for the imaginary part. Here we assume both the real and imaginary part are finite for the off-diagonal element of the input quantum state. Under this assumption,

the solution for ϕ can be casted as

$$\begin{aligned} \cos \phi^* &= \pm \frac{R}{\sqrt{R^2 + I^2}}, \\ \sin \phi^* &= \pm \frac{I}{\sqrt{R^2 + I^2}}. \end{aligned} \quad (\text{A4})$$

Then inserting the above solution for $\phi = \phi^*$ into Eq. (A1), we arrive

$$\rho'_{11}(\theta, \phi^*) = \frac{1}{2} + \frac{\rho_{11} - \rho_{22}}{2} \cos \theta \mp \sqrt{R^2 + I^2} \sin \theta, \quad (\text{A5})$$

and the off-diagonal element

$$\begin{aligned} \rho'_{12}(\theta, \phi^*, \omega) e^{i\omega} &= \frac{\rho_{11} - \rho_{22}}{2} \sin \theta - iR \sin \phi + iI \cos \phi \\ &\quad + R \cos \theta \cos \phi + I \cos \theta \sin \phi \\ &= \frac{\rho_{11} - \rho_{22}}{2} \sin \theta \pm \sqrt{R^2 + I^2} \cos \theta. \end{aligned} \quad (\text{A6})$$

Then derivative of ρ'_{11} in terms of θ , $\partial_\theta \rho'_{11} = 0$, leads to

$$\mp \sqrt{4R^2 + 4I^2} \cos \theta = (\rho_{11} - \rho_{22}) \sin \theta, \quad (\text{A7})$$

which results in

$$\begin{aligned} \cos \theta^* &= \pm \frac{\rho_{11} - \rho_{22}}{\sqrt{(\rho_{11} - \rho_{22})^2 + 4R^2 + 4I^2}}, \\ \sin \theta^* &= \pm \frac{\mp \sqrt{4R^2 + 4I^2}}{\sqrt{(\rho_{11} - \rho_{22})^2 + 4R^2 + 4I^2}}. \end{aligned} \quad (\text{A8})$$

Solutions for the ϕ^* and θ^* provides the result of ρ' at the extreme points with

$$\begin{aligned} \rho'_{11}(\theta^*, \phi^*) &= \frac{1}{2} \pm \frac{1}{2} \sqrt{(\rho_{11} - \rho_{22})^2 + 4R^2 + 4I^2} \\ &= \frac{1}{2} \pm \frac{1}{2} \sqrt{(\rho_{11} - \rho_{22})^2 + 4\rho_{12}\rho_{21}}, \\ \rho'_{12}(\theta^*, \phi^*, \omega) &= 0. \end{aligned} \quad (\text{A9})$$

Here $\rho'_{11}(\theta^*, \phi^*)$ equal to the eigenvalues of ρ through solving the characteristic equation $\det(\rho - \lambda I) = 0$.

Appendix B: Optimization with hardware-efficient quantum circuit

A universal parametrization for the N -qubit unitary transformation, as specified in Eq. (2), ensures the expressivity of the quantum circuit. For practical implementation, a hardware-efficient quantum circuit with finite depth is employed to represent the diagonal transformation matrix. To achieve this, we introduce a dynamic extension process for constructing the quantum circuit, utilizing a building block based on a brick-wall architecture. As illustrated in Fig. 5,

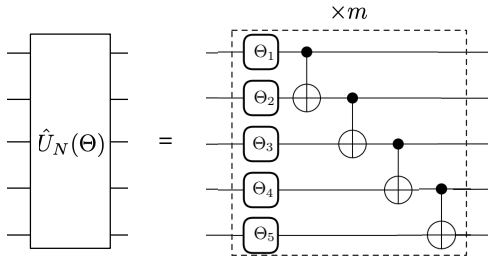


FIG. 5. For an $N = 5$ qubit system, the quantum circuit is constructed using m building blocks. As illustrated within the dashed box, the building block $\hat{\mathcal{B}}(\Theta)$ follows a brick-wall architecture.

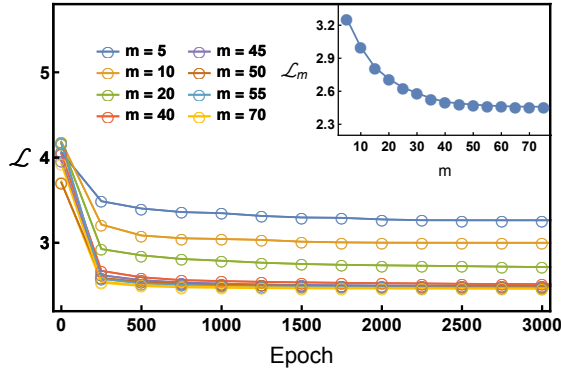


FIG. 6. Dynamic training process for a 5-qubit quantum state using the brick-wall building block. For each m , the objective function \mathcal{L} is plotted as a line with circular markers. The inset shows the minimal objective function \mathcal{L}_m obtained for each m .

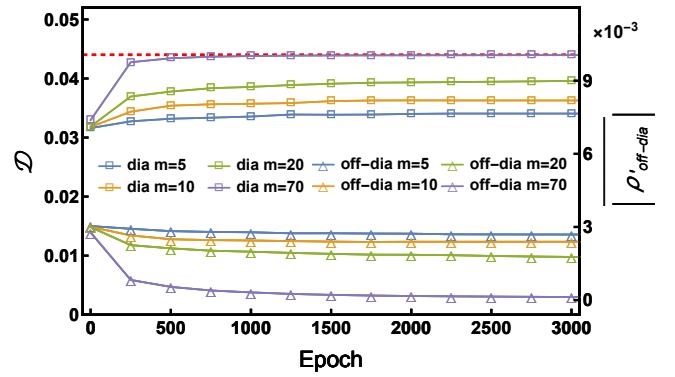


FIG. 7. For each m , the diagonal quantities \mathcal{D} and off-diagonal quantities $|\rho'_{\text{off-dia}}|$ are represented as shown as lines with triangular and square markers respectively. The red dashed line indicates the purity of the quantum state with 5 qubits.

the brick-wall building block, $\hat{\mathcal{B}}(\Theta)$, begins with N single-qubit gates, followed by $N - 1$ CNOT gates. The single-qubit gates are defined by the expression in Eq. (10), where each set of parameters Θ_q contains three elements: θ, ω and ϕ . This building block is then repeated m times to construct a variational quantum circuit, expressed as

$$\hat{U}_N(\Theta) = \Pi_{j=1}^m \hat{\mathcal{B}}(\Theta_j), \quad (\text{B1})$$

as shown in Fig. 5.

For $N = 5$, as shown in Fig. 6, we begin with a shallow quantum circuit, choosing $m = 5$ as an example. As training progresses, shown by the blue line with open circular markers, the objective function \mathcal{L} approaches its minimum value \mathcal{L}_m . As shown by the blue lines in Fig. 7, in the end of training for $m = 5$, the deviation of \mathcal{D} from the purity (red dashed line) exists due to the presence of finite off-diagonal elements. This indicates that the corresponding quantum circuit with $m = 5$ is too shallow to fully express the diagonal matrix. To address this, additional building blocks are incorporated into the circuit. Extension of the depth of the quantum circuit is repeated until \mathcal{L}_m is convergent, as shown in the inset of Fig. 6. For $N = 5$ and $m = 70$, as shown by the purple lines in Fig. 7, the off-diagonal elements of the evolved state become infinitesimally small. Meanwhile, \mathcal{D} saturates to the purity \mathcal{P} , confirming that the evolved state is diagonal.

* juanyao.physics@gmail.com

[1] Serge Lang. *Linear Algebra*. Undergraduate Texts in Mathematics. Springer New York, NY, 1987.
 [2] David J. Griffiths and Darrell F. Schroeter. *Introduction to Quantum Mechanics*. Cambridge University Press, third edition, 2018.
 [3] Christopher M. Bishop. *Pattern Recognition and Machine Learning*. Springer New York, NY, 2006.
 [4] Gene H. Golub and Charles F. Van Loan. *Matrix Computations*. Johns Hopkins University Press, 4th edition, 2013.

[5] Richard Bronson, Gabriel B. Costa, and John T. Saccoman. *Linear Algebra: Algorithms, Applications, and Techniques*. Academic Press, third edition, 2014.
 [6] Lloyd N. Trefethen and David Bau, III. *Numerical Linear Algebra*. Society for Industrial and Applied Mathematics, 1997.
 [7] William H. Press, Brian P. Flannery, Saul A. Teukolsky, and William T. Vetterling. *Numerical Recipes: The Art of Scientific Computing*. Cambridge University Press, 3rd edition, 2007.
 [8] Michael A. Nielsen and Isaac L. Chuang. *Quantum Computation and Quantum Information: 10th Anniversary Edition*.

Cambridge University Press, 2010.

- [9] Peter W. Shor. Algorithms for quantum computation: discrete logarithms and factoring. In *Proceedings 35th Annual Symposium on Foundations of Computer Science*, pages 124–134, 1994.
- [10] Peter W. Shor. Polynomial-time algorithms for prime factorization and discrete logarithms on a quantum computer. *SIAM Journal on Computing*, 26(5):1484–1509, 1997.
- [11] Seth Lloyd, Masoud Mohseni, and Patrick Rebentrost. Quantum principal component analysis. *Nature Physics*, 10(9):631–633, 2014.
- [12] Ryan LaRose, Arkin Tikku, Étude O’Neel-Judy, Lukasz Cincio, and Patrick J. Coles. Variational quantum state diagonalization. *npj Quantum Information*, 5(1):57, 2019.
- [13] Carlos Bravo-Prieto, Diego García-Martín, and José I. Latorre. Quantum singular value decomposer. *Phys. Rev. A*, 101:062310, Jun 2020.
- [14] M. Cerezo, Kunal Sharma, Andrew Arrasmith, and Patrick J. Coles. Variational quantum state eigensolver. *npj Quantum Information*, 8(1):113, 2022.
- [15] Akash Kundu, Przemysław Bedelek, Mateusz Ostaszewski, Onur Danaci, Yash J Patel, Vedran Dunjko, and Jarosław A Miszczak. Enhancing variational quantum state diagonalization using reinforcement learning techniques. *New Journal of Physics*, 26(1):013034, jan 2024.
- [16] M. Cerezo, Andrew Arrasmith, Ryan Babbush, Simon C. Benjamin, Suguru Endo, Keisuke Fujii, Jarrod R. McClean, Kosuke Mitarai, Xiao Yuan, Lukasz Cincio, and Patrick J. Coles. Variational quantum algorithms. *Nature Reviews Physics*, 3(9):625–644, 2021.
- [17] Sergey Bravyi, Graeme Smith, and John A. Smolin. Trading classical and quantum computational resources. *Phys. Rev. X*, 6:021043, Jun 2016.
- [18] Adam Paszke, Sam Gross, Francisco Massa, Adam Lerer, James Bradbury, Gregory Chanan, Trevor Killeen, Zeming Lin, Natalia Gimelshein, Luca Antiga, Alban Desmaison, Andreas Köpf, Edward Yang, Zach DeVito, Martin Raison, Alykhan Tejani, Sasank Chilamkurthy, Benoit Steiner, Lu Fang, Junjie Bai, and Soumith Chintala. PyTorch: An Imperative Style, High-Performance Deep Learning Library. arXiv:1912.01703.
- [19] Ville Bergholm, Josh Izaac, Maria Schuld, Christian Gogolin, Shahnawaz Ahmed, Vishnu Ajith, M. Sohaib Alam, Guillermo Alonso-Linaje, B. AkashNarayanan, Ali Asadi, Juan Miguel Arrazola, Utkarsh Azad, Sam Banning, Carsten Blank, Thomas R. Bromley, Benjamin A. Cordier, Jack Ceroni, Alain Delgado, Olivia Di Matteo, Amintor Dusko, Tanya Garg, Diego Guala, Anthony Hayes, Ryan Hill, Aroosa Ijaz, Theodor Isaacsson, David Ittah, Soran Jahangiri, Prateek Jain, Edward Jiang, Ankit Khandelwal, Korbinian Kottmann, Robert A. Lang, Christina Lee, Thomas Loke, Angus Lowe, Keri McKiernan, Johannes Jakob Meyer, J. A. Montañez-Barrera, Romain Moyard, Zeyue Niu, Lee James O’Riordan, Steven Oud, Ashish Panigrahi, Chae-Yeun Park, Daniel Polatajko, Nicolás Quesada, Chase Roberts, Nahum Sá, Isidor Schoch, Borun Shi, Shuli Shu, Sukin Sim, Arshpreet Singh, Ingrid Strandberg, Jay Soni, Antal Száva, Slimane Thabet, Rodrigo A. Vargas-Hernández, Trevor Vincent, Nicola Vitucci, Maurice Weber, David Wierichs, Roeland Wiersema, Moritz Willmann, Vincent Wong, Shaoming Zhang, and Nathan Killoran. PennyLane: Automatic differentiation of hybrid quantum-classical computations, July 2022. arXiv:1811.04968 [quant-ph].
- [20] <https://github.com/jy19Phy/VQSD>.
- [21] Juan Yao. Quantum state reconstruction via disentanglement with sequential optimization algorithm. *Machine Learning: Science and Technology*, 5(4):045027, oct 2024.
- [22] J. B. Altepeter, D. Branning, E. Jeffrey, T. C. Wei, P. G. Kwiat, R. T. Thew, J. L. O’Brien, M. A. Nielsen, and A. G. White. Ancilla-assisted quantum process tomography. *Phys. Rev. Lett.*, 90:193601, May 2003.
- [23] Daniel F. V. James, Paul G. Kwiat, William J. Munro, and Andrew G. White. Measurement of qubits. *Phys. Rev. A*, 64:052312, Oct 2001.
- [24] G. Mauro D’Ariano, Matteo G.A. Paris, and Massimiliano F. Sacchi. Quantum tomography. In Peter W. Hawkes, editor, *Quantum Tomography*, volume 128 of *Advances in Imaging and Electron Physics*, pages 205–308. Elsevier, 2003.
- [25] Yadong Wu, Pengfei Zhang, and Hui Zhai. Scrambling ability of quantum neural network architectures. *Phys. Rev. Res.*, 3:L032057, Sep 2021.
- [26] Yuxuan Du, Tao Huang, Shan You, Min-Hsiu Hsieh, and Dacheng Tao. Quantum circuit architecture search for variational quantum algorithms. *npj Quantum Information*, 8(1):62, 2022.
- [27] Further details can be found in Appendix B.
- [28] X. Mi, M. Sonner, M. Y. Niu, K. W. Lee, B. Foxen, R. Acharya, I. Aleiner, T. I. Andersen, F. Arute, K. Arya, A. Asfaw, J. Atalaya, J. C. Bardin, J. Basso, A. Bengtsson, G. Bortoli, A. Bourassa, L. Brill, M. Broughton, B. B. Buckley, D. A. Buell, B. Burkett, N. Bushnell, Z. Chen, B. Chiaro, R. Collins, P. Conner, W. Courtney, A. L. Crook, D. M. Debroy, S. Demura, A. Dunsworth, D. Eppens, C. Erickson, L. Faoro, E. Farhi, R. Fatemi, L. Flores, E. Forati, A. G. Fowler, W. Giang, C. Gidney, D. Gilboa, M. Giustina, A. G. Dau, J. A. Gross, S. Habegger, M. P. Harrigan, M. Hoffmann, S. Hong, T. Huang, A. Huff, W. J. Huggins, L. B. Ioffe, S. V. Isakov, J. Iveland, E. Jeffrey, Z. Jiang, C. Jones, D. Kafri, K. Kechedzhi, T. Khattar, S. Kim, A. Y. Kitaev, P. V. Klimov, A. R. Klots, A. N. Korotkov, F. Kostritsa, J. M. Kreikebaum, D. Landhuis, P. Laptev, K.-M. Lau, J. Lee, L. Laws, W. Liu, A. Locharla, O. Martin, J. R. McClean, M. McEwen, B. Meurer Costa, K. C. Miao, M. Mohseni, S. Montazeri, A. Morvan, E. Mount, W. Mruczkiewicz, O. Naaman, M. Neeley, C. Neill, M. Newman, T. E. O’Brien, A. Opremcak, A. Petukhov, R. Potter, C. Quintana, N. C. Rubin, N. Saei, D. Sank, K. Sankaragomathi, K. J. Satzinger, C. Schuster, M. J. Shearn, V. Shvarts, D. Strain, Y. Su, M. Szalay, G. Vidal, B. Villalonga, C. Vollgraff-Heidweiller, T. White, Z. Yao, P. Yeh, J. Yoo, A. Zalcman, Y. Zhang, N. Zhu, H. Neven, D. Bacon, J. Hilton, E. Lucero, R. Babbush, S. Boixo, A. Megrant, Y. Chen, J. Kelly, V. Smelyanskiy, D. A. Abanin, and P. Roushan. Noise-resilient edge modes on a chain of superconducting qubits. *Science*, 378(6621):785–790, 2022.
- [29] John Preskill. Quantum computing and the entanglement frontier. arXiv:1203.5813.
- [30] Aram W. Harrow and Ashley Montanaro. Quantum computational supremacy. *Nature*, 549(7671):203–209, 2017.